Volume extrapolation via eigenvector continuation

Nuwan Yapa[1,*] and Sebastian König[1,†]

[1] *Department of Physics, North Carolina State University, Raleigh, North Carolina 27695, USA*

We develop an extension of eigenvector continuation (EC) that makes it possible to extrapolate simulations of quantum systems in finite periodic boxes across large ranges of box sizes. The formal justification for this approach, which we call finite-volume eigenvector continuation (FVEC), is provided by matching periodic functions at different box sizes. As concrete FVEC implementation we use a discrete variable representation based on plane-wave states and present several applications calculated within this framework.

I. INTRODUCTION

Simulations of quantum systems in finite volume (FV), such as a cubic box with periodic boundary conditions, can be used to obtain information about that same system in infinite volume. In a series of highly influential papers [1–3], Lüscher has shown that the real-world (infinite-volume) properties of the system are encoded in how its (discrete) energy levels change as the size of the volume is varied. Bound-state relations connect the finite-volume energy correction to the asymptotic properties of wave functions, leading to an exponential volume dependence [1, 4–6], while information about elastic scattering can be obtained from discrete energy levels with power-law dependence on the box size. Resonances, *i.e.*, short-lived, unstable states, are manifest in the volume-dependent spectrum as avoided crossings of energy levels [7–9]. While early studies of finite-volume relations considered two-body applications, work in recent years has focused largely on deriving rigorous FV quantization conditions for three-body systems [10–22], following early studies of the triton and Efimov trimers in finite volume [23–26]. Related work has derived the volume dependence for bound states comprised of an arbitrary number of particles [6], and it has been demonstrated that genuine few-body resonances can be identified from FV calculations [27], thus providing a discovery tool for such exotic states.

Eigenvector continuation (EC), first introduced in Ref. [28], is a powerful (yet strikingly simple in practice) method to address otherwise unfeasible physics problems. Given a Hamiltonian with parametric dependence $H(c)$, EC enables robust extrapolations to a given target point c_* from "training data" far away from that point by exploiting information contained in eigenvectors. The essence of the system is "learned" through the construction of a highly effective (nonorthogonal) basis, leading to a variational calculation of the states of interest with rapid convergence [29]. Recent work [30, 31] has shown that EC as a particular reduced-basis (RB) method falls within a larger class of model-order reduction (MOR) techniques. In practice, EC boils down to constructing Hamiltonian and norm matrices (denoted as $H(c_*)$ and N, respectively) and solving the generalized eigenvalue problem $H(c_*)|\psi\rangle = \lambda N|\psi\rangle$.

Since its inception, various interesting applications and extensions of EC have been identified in a short time. Early applications focusing on bound states include the construction of highly efficient emulators for uncertainty quantification [32–34] and robust extrapolations of perturbation theory [35–37]. More recently, the approach has been extended to construct emulators for scattering systems [38–40] and to studies of nuclear reactions [41, 42].

We introduce here a novel extension of EC that goes beyond simple parametric dependencies of the Hamiltonian. Specifically, we develop EC as a tool for performing volume extrapolations at greatly reduced numerical cost. Since this extension is applicable in connection with any numerical method that provides access to wave functions in periodic finite topologies, it immediately yields several interesting applications, among which we highlight in particular FV studies of few-body resonances [27, 43]. Identifying such unstable states as avoided crossing of FV energy levels requires the calculation of spectra over a range of volumes, and in particular in very large boxes to reach, for example, the low-energy regime of few-neutron systems, which are of great current interest in nuclear experiments [44, 45] and nuclear theory (see, for example, Refs. [43, 46–48]). The technique introduced in this paper provides a way to greatly extend the reach of FV resonance studies. Moreover, few-body approaches used to extrapolate Lattice QCD results to infinite volume via matching to an effective field theory description, recently discussed in Ref. [49], can benefit from EC based volume extrapolation.

II. FINITE-VOLUME EIGENVECTOR CONTINUATION

By "finite-volume eigenvector continuation (FVEC)" we refer to the application of EC to extrapolate properties of quantum states calculated in a set of periodic boxes with sizes L_i, $i = 1, \cdots N$ to a target volume L_*. This should be distinguished from using standard EC at a fixed single volume L to extrapolate a parametric dependence of the Hamiltonian. Specifically, we want

* ysyapa@ncsu.edu
† skoenig@ncsu.edu

to consider states $|\psi_{L_i}\rangle$ at volume L_i (or sets of states $\{|\psi^{(j)}_{L_i}\rangle,\, j=1,\cdot\cdot N_i\}$) and perform EC using Hamiltonian and norm matrices

$$H_{ij} = \langle\psi_{L_i}|H_{L_*}|\psi_{L_j}\rangle\,, \tag{1a}$$
$$N_{ij} = \langle\psi_{L_i}|\psi_{L_j}\rangle\,. \tag{1b}$$

However, at face value the above definitions appear problematic because the dependence on L does not simply stem from the Hamiltonian; it is inherent in the definition of the Hilbert space. Two states $|\psi_{L_i}\rangle$ and $|\psi_{L_j}\rangle$ are actually vectors in different Hilbert spaces for $i \neq j$, and it is not immediately clear how the matrix elements written down naively in Eqs. (1) can be well-defined quantities. To resolve this issue, we develop the notion of a vector space that accommodates states with arbitrary periodicities and show how it relates to FVEC calculations.

A. Periodic matching

Let $\mathcal{H}_L$ be the space of periodic functions $f:\mathbb{R}\to\mathbb{C}$ with $f(x+L)=f(x)$ for some fixed but arbitrary $L>0$. Consider the union

$$\mathcal{H} = \bigcup_{\{L>0\}} \mathcal{H}_L\,. \tag{2}$$

We proceed to show that this concept can be used to define overlaps and matrix elements of periodic states with different periods. We restrict the discussion to the special case of a one-dimensional (1D) two-body system (described by a single relative coordinate x), and merely note that everything generalizes to a larger number of spatial dimensions and/or particles in a straightforward manner.

a. Addition. Clearly $\mathcal{H}$ is not a vector space if one defines the sum of $f,g\in\mathcal{H}$ in the usual pointwise manner (because the sum of two periodic functions is not in general periodic). However, for given $L,L'>0$ one can map $f\in\mathcal{H}_L$ to $\mathcal{H}_{L'}$ by means of a *dilatation*:

$$(D_{L,L'}f)(x) = \sqrt{\frac{L}{L'}}\, f\!\left(\frac{L}{L'}x\right)\,. \tag{3}$$

With this, we can define an addition operation for $f\in\mathcal{H}_L$ and $g\in\mathcal{H}_{L'}$ as follows:

$$(f \overset{\max}{+} g)(x) = (D_{L,L'}f)(x) + g(x) \tag{4}$$

for $L'>L$, and adjusting g instead in the opposite case. The result is a periodic function in $\mathcal{H}_{L'}\subset\mathcal{H}$, and since multiplication by a scalar is trivially defined, $(\mathcal{H}, \overset{\max}{+})$ is a vector space.

b. Inner products. An inner product on $\mathcal{H}$ can be defined similarly. Let $f,g\in\mathcal{H}$ and, without loss of generality, assume $L\le L'$ for the periods of f and g, respectively. Then

$$\langle f,g\rangle_{\max} = \langle D_{L,L'}f, g\rangle_{\mathcal{H}_{L'}} = \int_{-L'/2}^{L'/2} (D_{L,L'}f)(x)^* g(x)\,\mathrm{d}x \tag{5}$$

defines an inner product on $(\mathcal{H}, \overset{\max}{+})$. Indeed, consider for example adding $h\in\mathcal{H}_{L''}$ with $L''\ge L'$ to the second operand:

$$\begin{aligned}\langle f, g \overset{\max}{+} h\rangle_{\max} &= \langle f, D_{L',L''}g + h\rangle_{\max}\\ &= \langle D_{L,L''}f, D_{L',L''}g + h\rangle_{\mathcal{H}_{L''}}\\ &= \langle D_{L,L''}f, D_{L',L''}g\rangle_{\mathcal{H}_{L''}} + \langle D_{L,L''}f, h\rangle_{\mathcal{H}_{L''}}\\ &= \langle f,g\rangle_{\max} + \langle f,h\rangle_{\max}\,,\end{aligned} \tag{6}$$

where we set $x' = (L'/L'')x$ to find

$$\begin{aligned}&\langle D_{L,L''}f, D_{L',L''}g\rangle_{\mathcal{H}_{L''}}\\ &= \int_{-L''/2}^{L''/2} \sqrt{\frac{L}{L''}}\, f\!\left(\frac{L}{L''}x\right)^* \sqrt{\frac{L'}{L''}}\, g\!\left(\frac{L'}{L''}x\right)\,\mathrm{d}x\\ &= \int_{-L'/2}^{L'/2} \sqrt{\frac{L}{L'}}\, f\!\left(\frac{L}{L'}x'\right)^* g(x')\,\mathrm{d}x' = \langle f,g\rangle_{\max}\,.\end{aligned} \tag{7}$$

They key step above was using the property $D_{L,L''}f = D_{L,L'}D_{L',L''}f$ of dilatations (which actually form a multiplicative group). Other combinations of operands and periods work similarly, and again including scalar factors is trivial.

c. Matrix elements. Finally, consider a (linear) operator O on $\mathcal{H}_L$. While initially this is only given as a mapping $\mathcal{H}_L\to\mathcal{H}_L$, we can define its action on a function $f\in\mathcal{H}_{L'}$ by inserting an appropriate dilatation:

$$Of \equiv OD_{L',L}f \in \mathcal{H}_L\,. \tag{8}$$

Together with the inner product (5) this provides a definition of operator matrix elements between different $\mathcal{H}_L$, $\mathcal{H}_{L'}$.

B. Truncated periodic bases

Consider now truncated bases $S_{L,N}$ and $S_{L',N}$ for $\mathcal{H}_L$ and $\mathcal{H}_{L'}$, respectively, with N a positive integer. Specifically, let $S_{L,N} = \{\phi^{(L)}_j : j=1,\cdot\cdot N\}$ with

$$\phi^{(L)}_j(x) = \frac{1}{\sqrt{L}}\exp\left(\mathrm{i}\frac{2\pi j}{L}x\right) \tag{9}$$

be a set of plane waves. Then $D_{L,L'}$ is a bijection between $S_{L,N}$ and $S_{L',N}$, and because for each j we have $D_{L,L'}\phi^{(L)}_j = \phi^{(L')}_j$. Therefore, if ψ and ψ' are functions expanded upon $S_{L,N}$ and $S_{L',N}$, respectively, taking the inner product of their coefficient vectors in $\mathbb{R}^N$ is the same as considering the inner product on $\mathcal{H}$ as defined in Eq. (5). Note that while this inner product has been defined by matching functions to the maximum period, we

could equally well have chosen to match to the smaller period. In practice the concrete choice does not matter because both lead to identical inner products on $\mathbb{R}^N$. Overall we have arrived at a justification for writing down Eqs. (1) as well a straightforward prescription for implementing FVEC numerically.

Discrete variable representation. While conceptually straightforward, the plane-wave basis (9) is in general not an efficient approach to study few-body systems. It can, however, be used as starting point for the construction of a so-called discrete variable representation (DVR). Originally suggested as an alternative to harmonic-oscillator based calculations in nuclear physics [50], recent work has established this plane-wave DVR as a powerful numerical framework for studying few-body resonances in FV [27, 43, 51]. Its construction starts with the states $\phi_j(x)$ defined in Eq. (9), with $j = -N/2, \cdot\cdot N/2-1$ for even $N > 2$, and where as before x denotes the relative coordinate for a two-body ($n = 2$) system in $d = 1$ dimensions. Any periodic solution of the 1D Schrödinger equation can be expanded in terms of the $\phi_j(x)$, yielding a discrete Fourier transform (DFT). Given a set of equidistant points $x_k \in [-L/2, L/2)$ and weights $w_k = L/N$ (independent of k), DVR states are constructed as [52]

$$\psi_k(x) = \sum_{i=-N/2}^{N/2-1} \mathcal{U}^*_{ki}\phi_i(x)\,, \tag{10}$$

with $\mathcal{U}_{ki} = \sqrt{w_k}\phi_i(x_k)$ defining a unitary matrix. Calculations in a periodic box can then be carried out through an expansion in terms of the $\psi_k(x)$ instead of the $\phi_j(x)$. Importantly, since the transformation between plane-wave states and DVR states is unitary, the above considerations that justify FVEC carry over to DVR calculations.

Local potentials are represented in the DVR by basis diagonal matrices [27, 51]. Separable potentials have a more complicated representation, but can also be implemented efficiently [43]. Another advantage of the DVR is that despite being effectively defined on a lattice of points, it yields a continuum dispersion relation $E = p^2/(2\mu)$, where p and μ are the center-of-mass momentum and the reduced mass of the system, respectively. This is achieved by a nondiagonal matrix representation for the kinetic energy K, which is, however, known analytically [27, 51]. For $d > 1$ or $n > 2$ the DVR representation of K becomes a sparse matrix that can be calculated very efficiently based only on the 1D two-body matrix elements. The DVR construction in this case starts from product states of $(n-1)\times d$ plane waves.

As discussed in Refs. [27, 51] it is straightforward (and numerically very efficient) to construct out of these basic states subspaces with proper bosonic or fermionic (including spin degrees of freedom) symmetry properties, and, optionally, definite parity. Moreover, the breaking of spherical symmetry in infinite volume down to the cubic symmetry subgroup O in FV can be accounted for by introducing appropriate projectors [53], represented as sparse matrices in the DVR basis [27]. These projectors select a specific cubic irreducible representation Γ out of the set $\{A_1, A_2, E, T_1, T_2\}$ (with dimensionalities 1, 1, 2, 3, and 3, respectively). Angular-momentum multiplets are reducible with respect to O, so each angular-momentum state in infinite volume in general contributes to several Γ. Low-lying A_1 states are to a good approximation dominated by infinite-volume S-wave states, whereas P-wave states contribute predominantly to T_1 multiplets. In practice it suffices to perform cubic-projected calculations at selected volumes in order to assign quantum numbers.

III. APPLICATIONS

A. Simple two-body system

As a first test we consider a simple two-body system (in three dimensions) interacting via a Gaussian potential

$$V(r) = V_0 \exp\left(-\left(\frac{r}{R}\right)^2\right). \tag{11}$$

For this calculation we use natural units with $\hbar = c = 1$ and also set the particle mass $m = 1$. As (arbitrary) specific choice we set $R = 2$ and $V_0 = -4.0$, which produces a spectrum with two bound S-wave states in infinite volume, one of which is very loosely bound. In finite volume both bound states are found in the A_1^+ representation, where the superscript indicates positive parity. The FV spectrum including the lowest states is shown in Fig. 1. For the FVEC calculation we chose to include training data at four different volumes, $L = 6, 7, 8, 9$, including four states at each training volume so that the total number of training data is $4 \times 4 = 16$. This covers the two A_1^+ bound states as well as the lowest lying scattering states, falling in the two-fold degenerate E^+ representation. The DVR calculation was performed using an $N = 32$ model space for all data points. Extrapolation based on this training set work very well, as shown in Fig. 1 up to $L = 20$, with merely about 4% deviation between FVEC and exact calculation for the ground state at $L = 20$.

B. Three-boson resonance

As another application we consider three identical spin-0 bosons with mass $m = 939.0$ MeV (mimicking neutrons) interacting via the two-body potential

$$V(r) = V_0 \exp\left(-\left(\frac{r}{R_0}\right)^2\right) + V_1 \exp\left(-\left(\frac{r-a}{R_1}\right)^2\right), \tag{12}$$

with $V_0 = -55$ MeV, $V_1 = 1.5$ MeV, $R_0 = \sqrt{5}$ fm, $R_1 = 10$ fm, and $a = 5$ fm. This potential produces

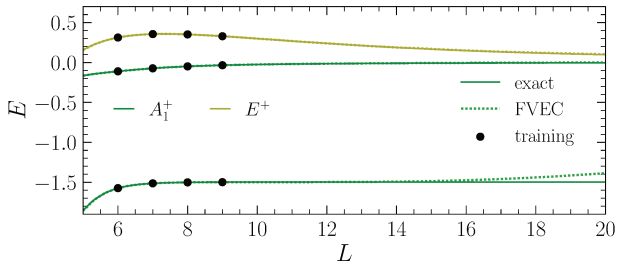

Figure 1. Positive-parity energy spectrum of two particles in finite volume as a function of the box size L for a Gaussian potential (11) with $R = 2$ and $V_0 = -4.0$ in natural units (see text). Solid lines show the three lowest energy levels calculated in a DVR basis with $N = 32$. Dashed lines indicate FVEC results obtained based on training data from four different box sizes (solid circles).

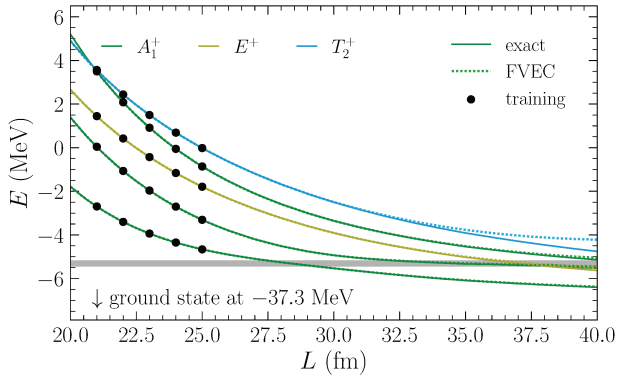

Figure 2. Positive-parity finite-volume energy spectrum of three bosons interacting via the potential (12). Solid lines show the exact states calculated in DVR bases with $N \leq 28$, whereas dashed lines indicate FVEC results obtained based on training data at five different box sizes (solid circles). The FVEC calculation was performed using $8 \times 5 = 40$ training states, which includes the A_1^+ ground state not shown in the plot. See text for details.

a resonance state with energy $E_R = -5.31$ MeV and half width 0.12 MeV [54] (shaded band in Fig. 2).

In Fig. 2 we show an FVEC calculation for this system, using training data at five different box sizes $L = 21, 22, 23, 24, 25$ fm with $N = 28$. For each training volume eight states were included, covering four A_1^+ states (including the deeply bound ground state not shown in the figure), one E^+ state, and one T_2^+ state (for which only part of cubic multiplet was included because the training calculations did not all yield the full triplet). In total, $8 \times 5 = 40$ training states were included. The FVEC calculation provides an excellent reproduction of the exact energy levels, with noticeable deviations only for excited states at box sizes far away from the training regime. In particular, FVEC perfectly captures the avoided crossing between the lowest two A_1^+ states in Fig. 2, indicating the three-boson resonance that Ref. [27] extracted at $E_R = -5.32(1)$ MeV from the FV spectrum,

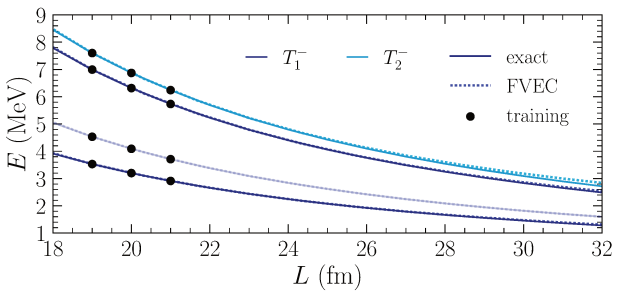

Figure 3. Negative-parity $S_z = 1/2$ finite-volume energy spectrum of three neutrons interacting via a separable contact potential fit to reproduce the neutron-neutron scattering length $a_{nn} = -18.9$ fm. Solid lines show the exact states calculated in DVR bases with $N \leq 22$, whereas dashed lines indicate FVEC results obtained based on $N = 22$ training data at three different box sizes (solid circles). The first and third levels shown in the plots are T_1^- states with total spin $S = 1/2$. The second level is a (noninteracting) $S = 3/2$ T_1^- state, whereas the fourth level is a T_2^- state with $S = 1/2$. A total number of $3 \times 8 = 24$ training data were used to generate this plot, covering a subset of states from the four three-dimensional multiplets (see text for details).

in good agreement with Ref. [54].

C. Three neutrons

Finally, we consider a system of three neutrons (n) in pionless effective field theory at leading order. Specifically, we use a separable momentum-space contact interaction,

$$V(q, q') = C\, g(q) g(q')\,, \tag{13}$$

where $g(q) = \exp(-q^{2n}/\Lambda^{2n})$ is a super-Gaussian regulator. A projector ensures that the potential acts only on spin-singlet neutron pairs with vanishing angular momentum (FV analog of the ${}^1S_0$ channel). This system was recently studied in Ref. [43] (which also discusses the use of separable interactions with the plane-wave DVR), and as in that work we set $n = 2$ and fix the momentum cutoff $\Lambda = 250$ MeV. The low-energy constant C is fixed to reproduce the nn scattering length $a_{nn} = -18.9$ fm.

Figure 3 shows results using training data from $N = 22$ DVR calculations at $L = 19, 20, 21$ fm. The DVR basis $\mathcal{B}$ was restricted to include only states with spin projection $S_z = 1/2$, which covers total spin $S = 1/2$ and $S = 3/2$. Its dimension $\dim \mathcal{B} = 28,344,960$ is quite sizable, and even larger bases are needed to converge the calculation in boxes with $L \geq 32$ fm [43]. Compared to the previous examples, this application is more involved because *(a)* the inclusion of spin increases the DVR basis size at fixed N and *(b)* the low-lying fermion spectrum is comprised of negative-parity T_1 and T_2 states, each coming as threefold degenerate multiplets (with dominant correspondence to P-wave and D-wave states in infinite

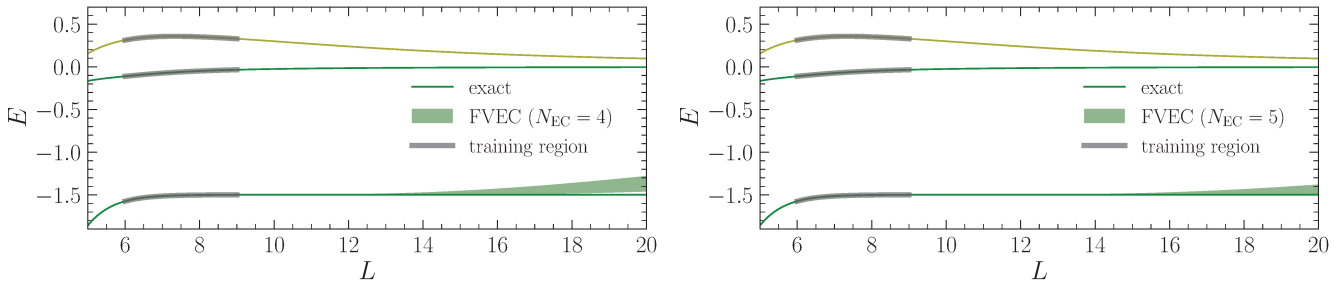

Figure 4. FVEC calculation with uncertainty estimates for two particles interacting via a Gaussian potential with range $R = 2$ and depth $V_0 = -4.0$ (in natural units). A pool of 16 training data sets with $6 \leq L \leq 9$ (indicated as dark shaded bands) was used to estimate the FVEC uncertainty by considering all combinations of $N_{\mathrm{EC}} = 4$ (left panel) and $N_{\mathrm{EC}} = 5$ (right panel) out of the overall pool. The range of all these individual calculations is shown as shaded bands.

volume, respectively). For the training calculations used to generate Fig. 3, the iterative diagonalization did not resolve all these degeneracies, finding between one and three states of each multiplet, not uniform across the different training volumes. In spite of these imperfections, FVEC still performs remarkably well after preprocessing the set of training vectors with a modified Gram-Schmidt orthogonalization. This step is well known to be useful for EC calculations in order to avoid numerical problems stemming from singular and/or ill-conditioned norm matrices. Therefore, this example demonstrates the robustness of the FVEC method.

IV. UNCERTAINTY ESTIMATION

The accuracy of an FVEC calculation depends on the choice of training data, both on the range it is chosen from and on the number of training points used to construct the EC subspace. This dependence can be used to estimate the inherent uncertainty in an FVEC prediction, which we illustrate in Fig. 4 for the same two-body system with attractive Gaussian interaction considered in Sec. III A. Instead of using a single fixed set of training points, we calculate (using $N = 32$ for the DVR calculation) a training pool of 16 box sizes located uniformly within the interval $6 \leq L \leq 9$. To generate the left panel in Fig. 4, we then pick all possible combinations of $N_{\mathrm{EC}} = 4$ training points out of this pool and perform an FVEC calculation for each of these combinations. The range of results from these calculations (performed for each target volume) is shown as shaded bands in Fig. 4. To generate the right panel in the figure the procedure was repeated choosing all combinations of $N_{\mathrm{EC}} = 5$ training points out of the pool of 16.

Accuracy and precision of the extrapolation evidently increase with higher N_{EC} as expected. The band for the ground state almost overlaps at large L with the exact result for $N_{\mathrm{EC}} = 5$, whereas the other levels are already well converged with $N_{\mathrm{EC}} = 4$ (so much so that the shaded bands for the excited states are barely visible in the figure). We note that due to the variational nature of EC calculations the bands always lie above the exact energy levels. This is a particular feature of energy observables, while no such constraint holds in general for expectation values of other operators [32].

V. DISCUSSION AND OUTLOOK

The examples considered above demonstrate that FVEC is able to perform well for a variety of different scenarios, including bound and unbound states and bosonic as well as fermionic systems. In particular, we find the performance of FVEC roughly independent of the dimension of the model space, considering that all applications above use comparable numbers of training data. Based on this one should expect FVEC to work equally well even at large scales.

Eigenvector continuation has built a reputation of yielding substantial speedups over exact calculations, to an extent that it can render possible otherwise unfeasible analyses [33]. FVEC does not disappoint in this regard: for example, an exact calculation at a single box size shown in Fig. 2 requires roughly 1100 matrix-vector multiplications to find the low-energy spectrum of the $N = 28$ DVR Hamiltonian using PARPACK [55]. The FVEC calculation with 40 training data points on the other hand requires only 40 such matrix-vector products (plus negligible numerical cost from vector-vector products and solving the EC eigenvalue problem). Since the cost of constructing the DVR Hamiltonian for each target box size is also comparatively negligible, FVEC provides a speedup factor of roughly 28 for a single L in this particular scenario, and even more for a calculation spanning multiple L such as shown in Fig. 2.

While the focus in the examples we presented has been on using FVEC for *extra*polation, there is no requirement to choose training data from a narrow set of volumes. Sampling instead on both ends of the regime of interest to perform an interpolation can further improve the accuracy of FVEC at fixed cost. Uncertainty estimation as discussed in Sec. IV works the same way for this scenario.

Our work provides a perspective for further extensions

of EC to scenarios where the parametric dependence is in the model space rather than just the Hamiltonian. In particular, it would be interesting to develop a version of EC to extrapolate the frequency parameter $\hbar\omega$ in calculations employing truncated harmonic-oscillator (HO) bases, which play an important role in nuclear physics. Such a scheme could for example leverage existing IR and UV extrapolation schemes [56–60].

ACKNOWLEDGMENTS

We thank Dean Lee, Pablo Giuliani, Edgard Bonilla, and Kyle Godbey for useful discussions and valuable comments on the manuscript. This work was supported in part by the National Science Foundation under Grant No. PHY–2044632. This material is based upon work supported by the U.S. Department of Energy, Office of Science, Office of Nuclear Physics, under the FRIB Theory Alliance, Award No. DE-SC0013617. Computational resources for parts of this work were provided by the Jülich Supercomputing Center. Moreover, we acknowledge computing resources provided on Henry2, a high-performance computing cluster operated by North Carolina State University.

[1] M. Lüscher, Comm. Math. Phys. **104**, 177 (1986).
[2] M. Lüscher, Comm. Math. Phys. **105**, 153 (1986).
[3] M. Lüscher, Nucl. Phys. B **354**, 531 (1991).
[4] S. König, D. Lee, and H.-W. Hammer, Phys. Rev. Lett. **107**, 112001 (2011).
[5] S. König, D. Lee, and H.-W. Hammer, Annals Phys. **327**, 1450 (2012).
[6] S. König and D. Lee, Phys. Lett. B **779**, 9 (2018).
[7] U.-J. Wiese, Nucl. Phys. B Proc. Suppl. **9**, 609 (1989).
[8] M. Lüscher, Nuclear Physics B **364**, 237 (1991).
[9] K. Rummukainen and S. Gottlieb, Nucl. Phys. B **450**, 397 (1995).
[10] K. Polejaeva and A. Rusetsky, Eur. Phys. J. A **48**, 67 (2012), arXiv:1203.1241 [hep-lat].
[11] R. A. Briceno and Z. Davoudi, Phys. Rev. D **87**, 094507 (2013), arXiv:1212.3398 [hep-lat].
[12] M. T. Hansen and S. R. Sharpe, Phys. Rev. D **92**, 114509 (2015), arXiv:1504.04248 [hep-lat].
[13] H.-W. Hammer, J.-Y. Pang, and A. Rusetsky, Journal of High Energy Physics **2017**, 109 (2017).
[14] H.-W. Hammer, J.-Y. Pang, and A. Rusetsky, Journal of High Energy Physics **2017**, 115 (2017).
[15] M. Mai and M. Döring, Eur. Phys. J. A **53**, 240 (2017), arXiv:1709.08222 [hep-lat].
[16] M. Döring, H.-W. Hammer, M. Mai, J.-Y. Pang, A. Rusetsky, and J. Wu, Phys. Rev. D **97**, 114508 (2018), arXiv:1802.03362 [hep-lat].
[17] J.-Y. Pang, J.-J. Wu, H.-W. Hammer, U.-G. Meißner, and A. Rusetsky, Phys. Rev. D **99**, 074513 (2019), arXiv:1902.01111 [hep-lat].
[18] C. Culver, M. Mai, R. Brett, A. Alexandru, and M. Döring, Phys. Rev. D **101**, 114507 (2020), arXiv:1911.09047 [hep-lat].
[19] R. A. Briceño, M. T. Hansen, S. R. Sharpe, and A. P. Szczepaniak, Phys. Rev. D **100**, 054508 (2019), arXiv:1905.11188 [hep-lat].
[20] F. Romero-López, S. R. Sharpe, T. D. Blanton, R. A. Briceño, and M. T. Hansen, Journal of High Energy Physics **2019**, 7 (2019).
[21] M. T. Hansen, F. Romero-López, and S. R. Sharpe, Journal of High Energy Physics **2020**, 47 (2020), [Erratum: JHEP 02, 014 (2021)].
[22] F. Müller, J.-Y. Pang, A. Rusetsky, and J.-J. Wu, Journal of High Energy Physics **2022**, 158 (2022).
[23] S. Kreuzer and H.-W. Hammer, Phys. Lett. B **694**, 424 (2011), arXiv:1008.4499 [hep-lat].
[24] S. Kreuzer and H. W. Grießhammer, Eur. Phys. J. A **48**, 93 (2012), arXiv:1205.0277 [nucl-th].
[25] S. Kreuzer and H.-W. Hammer, in *Proceedings, 5th Asia-Pacific Conference on Few-Body Problems in Physics 2011 (APFB2011): Seoul, Korea, August 22-26, 2011*, Vol. 54 (2013) pp. 157–164.
[26] U.-G. Meißner, G. Ríos, and A. Rusetsky, Phys. Rev. Lett. **114**, 091602 (2015), [Erratum: Phys. Rev. Lett.117 069902 (2016)], arXiv:1412.4969 [hep-lat].
[27] P. Klos, S. König, H.-W. Hammer, J. E. Lynn, and A. Schwenk, Phys. Rev. C **98**, 034004 (2018).
[28] D. Frame, R. He, I. Ipsen, D. Lee, D. Lee, and E. Rrapaj, Phys. Rev. Lett. **121**, 032501 (2018).
[29] A. Sarkar and D. Lee, Phys. Rev. Lett. **126**, 032501 (2021).
[30] E. Bonilla, P. Giuliani, K. Godbey, and D. Lee, (2022), arXiv:2203.05284 [nucl-th].
[31] J. A. Melendez, C. Drischler, R. J. Furnstahl, A. J. Garcia, and X. Zhang, (2022), arXiv:2203.05528 [nucl-th].
[32] S. König, A. Ekström, K. Hebeler, D. Lee, and A. Schwenk, Physics Letters B **810**, 135814 (2020).
[33] A. Ekström and G. Hagen, Phys. Rev. Lett. **123**, 252501 (2019).
[34] A. Sarkar and D. Lee, Phys. Rev. Research **4**, 023214 (2022).
[35] P. Demol, T. Duguet, A. Ekström, M. Frosini, K. Hebeler, S. König, D. Lee, A. Schwenk, V. Somà, and A. Tichai, Phys. Rev. C **101**, 041302 (2020).
[36] P. Demol, M. Frosini, A. Tichai, V. Somà, and T. Duguet, Annals Phys. **424**, 168358 (2021).
[37] M. Companys Franzke, A. Tichai, K. Hebeler, and A. Schwenk, Physics Letters B **830**, 137101 (2022).
[38] R. J. Furnstahl, A. J. Garcia, P. J. Millican, and X. Zhang, Phys. Lett. B **809**, 135719 (2020).
[39] J. A. Melendez, C. Drischler, A. J. Garcia, R. J. Furnstahl, and X. Zhang, Physics Letters B **821**, 136608 (2021).
[40] X. Zhang and R. J. Furnstahl, Phys. Rev. C **105**, 064004 (2022).
[41] C. Drischler, M. Quinonez, P. G. Giuliani, A. E. Lovell,

and F. M. Nunes, Phys. Lett. B **823**, 136777 (2021).
[42] D. Bai and Z. Ren, Phys. Rev. C **103**, 014612 (2021).
[43] S. Dietz, H.-W. Hammer, S. König, and A. Schwenk, Phys. Rev. C **105**, 064002 (2022).
[44] K. Kisamori, S. Shimoura, H. Miya, S. Michimasa, S. Ota, M. Assie, H. Baba, T. Baba, D. Beaumel, M. Dozono, T. Fujii, N. Fukuda, S. Go, F. Hammache, E. Ideguchi, N. Inabe, M. Itoh, D. Kameda, S. Kawase, T. Kawabata, M. Kobayashi, Y. Kondo, T. Kubo, Y. Kubota, M. Kurata-Nishimura, C. S. Lee, Y. Maeda, H. Matsubara, K. Miki, T. Nishi, S. Noji, S. Sakaguchi, H. Sakai, Y. Sasamoto, M. Sasano, H. Sato, Y. Shimizu, A. Stolz, H. Suzuki, M. Takaki, H. Takeda, S. Takeuchi, A. Tamii, L. Tang, H. Tokieda, M. Tsumura, T. Uesaka, K. Yako, Y. Yanagisawa, R. Yokoyama, and K. Yoshida, Phys. Rev. Lett. **116**, 052501 (2016).
[45] T. Faestermann, A. Bergmaier, R. Gernhäuser, D. Koll, and M. Mahgoub, Phys. Lett. B **824**, 136799 (2022).
[46] S. Gandolfi, H. W. Hammer, P. Klos, J. Lynn, and A. Schwenk, Phys. Rev. Lett. **118**, 232501 (2017), arXiv:1612.01502 [nucl-th].
[47] M. D. Higgins, C. H. Greene, A. Kievsky, and M. Viviani, Phys. Rev. C **103**, 024004 (2021), arXiv:2011.11687 [nucl-th].
[48] S. Ishikawa, Phys. Rev. C **102**, 034002 (2020), arXiv:2008.10980 [nucl-th].
[49] W. Detmold and P. E. Shanahan, Phys. Rev. D **103**, 074503 (2021).
[50] A. Bulgac and M. M. Forbes, Phys. Rev. C **87**, 051301 (2013).
[51] S. König, Few-Body Syst. **61**, 20 (2020).
[52] G. C. Groenenboom, "The Discrete Variable Representation," (2001).
[53] R. C. Johnson, Phys. Lett. B **114**, 147 (1982).
[54] J. Blandon, V. Kokoouline, and F. Masnou-Seeuws, Phys. Rev. A **75**, 042508 (2007).
[55] K. J. Maschhoff and D. C. Sorensen, "P_ARPACK: An Efficient Portable Large Scale Eigenvalue Package for Distributed Memory Parallel Architectures," `www.caam.rice.edu/software/ARPACK/`, `github.com/opencollab/arpack-ng`.
[56] S. N. More, A. Ekström, R. J. Furnstahl, G. Hagen, and T. Papenbrock, Phys. Rev. C **87**, 044326 (2013).
[57] R. J. Furnstahl, S. N. More, and T. Papenbrock, Phys. Rev. C **89**, 044301 (2014).
[58] S. König, S. K. Bogner, R. J. Furnstahl, S. N. More, and T. Papenbrock, Phys. Rev. C **90**, 064007 (2014).
[59] R. J. Furnstahl, G. Hagen, T. Papenbrock, and K. A. Wendt, J. Phys. G: Nucl. Part. Phys. **42**, 034032 (2015).
[60] K. A. Wendt, C. Forssén, T. Papenbrock, and D. Sääf, Phys. Rev. C **91**, 061301 (2015).